Effects of Unsaturation and Curvature on the Transverse Distribution of Intramolecular Dynamics of Dipyrenyl Lipids

Kwan Hon Cheng* and Pentti Somerharju‡
*Department of Physics, Texas Tech University, Lubbock, Texas 79409-1051 USA, and ‡Department of Medical Chemistry, Institute of Biomedicine, University of Helsinki, 00014 Helsinki, Finland

ABSTRACT The roles of acyl chain unsaturation and curvature in the excimer formation efficiency (EFE) of site-specific conjugated pyrene molecules in lipid membranes have been investigated by steady-state and time-resolved fluorescence spectroscopy. Six 1-2-(pyrenyl-*n*-acyl)-phosphatidylcholine (dipy$_n$PC) probes, with pyrenyl chains of varying methylene units *n* from 4 to 14 carbons, were incorporated separately into dioleoylphosphatidylcholine (DOPC) or dioleoylphosphatidylethanolamine (DOPE) lipid membranes at 0.1 mol %. Both the excimer-to-monomer fluorescence intensity ratio and association-to-dissociation rate constant ratio of conjugated pyrenes were used to quantify EFE. At all temperatures (T = 0–30°C) and for n = 4 and 6, the EFE for DOPE was always smaller than EFE for DOPC. At $T < 10$°C (where DOPE and DOPC are in the liquid crystalline L_α phase) and for $n > 8$, the EFE for curvature frustrated DOPE was significantly greater than EFE for nonfrustrated DOPC (control), and the difference increased gradually with n. At $T > 18$°C (where DOPE is in the inverted hexagonal H_{II} phase and DOPC is in the L_α phase) and for $n > 8$, EFE for the curvature-relaxed DOPE was again smaller than the EFE for DOPC control. The contributions of splay conformation and internal dynamics of pyrenyl chains to EFE were examined separately using a lattice model. Our results suggest that i) the *cis* double bonds of the host lipid matrix strongly perturb both the conformation and dynamics of conjugated pyrenes at the specific location around n = 8, and ii) the lateral stress at the upper part ($n < 8$) of the curvature frustrated bilayer membranes (DOPE) may be significantly relaxed once the membrane surface adopts a favorable negative interfacial curvature.

INTRODUCTION

The roles of structural conformations, dynamics, and interactions of self-assembling lipid molecules in various membrane-related properties and functions, e.g., phase transitions (Lafleur et al., 1990; Lewis et al., 1994), lipid-protein interactions (Heimburg et al., 1991; Slater et al., 1994), transport (Keller et al., 1993), curvature elasticity (Winterhalter and Helfrich, 1992), and fusion (Lentz et al., 1992), have been recognized for many years. However, site-specific molecular mechanisms, e.g., how the lipid molecules in bilayer membranes interact with other membrane components at specific locations and express the membrane-associated properties and functions (Gruner, 1992; Hui, 1993; Cheng et al., 1994a), are still speculative. Because of the highly anisotropic, amphiphilic, and heterogeneous nature of biological membranes, a better understanding of the structural conformation and dynamics of site-specific molecules in well-defined membranes is still required.

Recent structural measurements, e.g., x-ray and neutron diffraction (Wiener and White, 1992), and nuclear magnetic resonance (NMR) relaxation measurements (Fenske et al., 1990; Lafleur et al., 1990; Thurmond et al., 1993) have revealed fine conformational and relaxation details of lipid acyl chains, with spatial resolution on the order of methylene units (m.u.). Parallel theoretical investigations, e.g., molecular dynamics simulations (De Loof et al., 1991; Pearce and Harvey, 1993; Xiang, 1993; Fattal and Ben-Shaul, 1994; Chiu et al., 1995), have further provided insight into the arrangement and relaxation behavior of acyl chains at the subnanosecond scale. More detailed and systematic investigations of the molecular dynamic behavior of site-specific molecules in lipid membranes of well-defined acyl chain and headgroup compositions is needed. The site-specific information should be useful in understanding the delicate roles of lipid acyl chain interactions with membrane components, lipids, and proteins at defined locations, and the structural stability of membranes at the molecular level. This paper focuses on the effects of *cis* double bonds and curvature of the membranes on the transverse (along the normal of the membrane surface) distributions of excimer formation efficiency (EFE), as well as the splay conformation and internal mobilities of conjugated pyrene molecules of site-specific dipyrenyl lipids in unsaturated membranes of well-defined compositions.

The influence of double bonds on the transverse distribution of structural arrangement (order parameter) of acyl chains has been investigated by NMR (Seelig and Waespe-Šarčević, 1978). Basically, the presence of double bonds produces a significant local perturbation of the order parameter near the site of the double bonds within the NMR time scale. Recent theoretical investigations further support this observation (Rey et al., 1992; Fattal and Ben-Shaul, 1994). However, the effects of double bonds on the splay conformation and internal dynamics of site-selective mole-

Received for publication 22 November 1995 and in final form 7 February 1996.

Address reprint requests to Dr. Kwan-Hon Cheng, Biophysics Laboratory, Department of Physics, Texas Tech University, Box 41051, Lubbock, Texas 79409-1051. Tel.: 806-742-2992; Fax: 806-742-1182; E-mail: vckhc@ttacs.ttu.edu.

0006-3495/96/05/2287/12 $2.00

cules in the nanosecond fluorescence time scale are still unclear.

The roles of intrinsic (or spontaneous) curvature and interfacial curvature of lipid layers in the physical properties and specific membrane activities have been proposed (Gruner, 1992; Hui, 1993; Keller et al., 1993). Unsaturated phosphatidylethanolamine (PE) is a major phospholipid species found in eukaryotic cell membranes. PE has a small headgroup cross-sectional area relative to the hydrocarbon volume. Moreover, its headgroup is poorly hydrated and capable of forming interlipid hydrogen bonding at the lipid/water interface (Epand, 1995, and references therein). Therefore, PE containing monolayer possesses a large spontaneous curvature in bilayer membranes and tends to adopt nonbilayer phases with negative interfacial curvature at physiological conditions (Israelachvilli et al., 1977). On the other hand, phosphatidylcholine (PC), another major phospholipid species, has a larger and much more hydrated choline headgroup. Hence, PC remains in stable bilayer phase under similar physiological conditions. In symmetric bilayer containing PE, the tendency or propensity of PE to adopt nonbilayer structure is prevented by opposing forces of various origins, e.g., packing constraints and hydration, and thereby leads to curvature (or bending) frustration or the development of spontaneous curvature-related lateral stress (Seddon, 1990; Gruner, 1992). A systematic investigation of the transverse distributions of intramolecular dynamics of site-selective molecules in curvature frustrated and curvature-relaxed membranes is still lacking.

Free or conjugated planar pyrene molecules display concentration-dependent excimer fluorescence (Birks et al., 1963; Vauhkonen et al., 1990). Pyrene-labeled phospholipids have been widely used to study various membrane-related phenomena, e.g., lipid lateral diffusion (Galla and Hartmann, 1980; Vauhkonen et al., 1990), phospholipid conformation (Eklund et al., 1992; Sassaroli et al., 1995), and lateral organizations in lipid bilayers (Hresko et al., 1987; Tang and Chong, 1992). More recently, dipyrenyl lipids, in which both acyl chains are labeled with pyrene moieties, have also been used to determine the conformation and dynamics of phospholipid acyl chains from steady-state and kinetic (time-resolved) measurements of excimer formation (Vauhkonen et al., 1990; Sassaroli et al., 1993; Cowsley et al., 1993; Cheng et al., 1994a,b). In this study, dipyrenyl lipid species with acyl chain lengths varying from 4 to 14 methylene units were incorporated separately into neat dioleoyl PE (DOPE) membranes. By systematically varying the length of the pyrene-labeled chains, EFE, as well as the splay conformation and internal motions, of conjugated pyrenes at various depths in the host lipid matrix can be estimated from measurements of the excimer-to-monomer intensity ratio (E/M) and intensity decays of the pyrene monomer and excimer fluorescence (Cheng et al., 1994a,b). Parallel experiments were carried out with dioleoyl PC (DOPC) membranes. Here the acyl chain compositions of DOPE and DOPC are identical. By comparing the fluorescence data obtained from two different membranes, phospholipid-specific properties can be more clearly resolved than by studying a singe membrane system alone. The major goal of this study was to quantify the effect of localized double bonds and curvature on the transverse distributions of the EFE, as well as the conformation and dynamics, of site-selective molecules in membranes.

MATERIALS AND METHODS

Sample preparations

1,2-Dioleoylphosphatidylcholine (DOPC) and 1,2-dioleoylphosphatidylethanolamine (DOPE) in chloroform were purchased from Avanti Polar Lipids (Birmingham, AL) and used without further purification. Single-chain pyrene-labeled lipids, 1-palmitoyl-2-(pyrene-*n*-acyl)-phosphatidylcholine (pyr_nPC), and dual-chain pyrene-labeled lipids, 1–2-(pyrenyl-*n*-acyl)-phosphatidylcholine ($dipy_nPC$), of different chain lengths (methylene units n = 4, 6, 8, 10, 12, and 14) were synthesized by methods described previously (Vauhkonen et al., 1990). Pyr_nPC and $dipy_nPC$ were mixed with either DOPC or DOPE in chloroform at the molar ratios of 0.05% and 0.1%, respectively. The mixtures were dried under nitrogen gas and then kept under vacuum for at least 5 h. The dry lipid films were subsequently hydrated in an aqueous buffer (100 mM NaCl/10 mM *N*-tris-(hydroxymethyl) methyl-2-aminoethanesulfonic acid (TES)/2 mM EDTA, pH 7.4) at 0°C under mild sonication for a few seconds to assist the dispersion of the lipids. Thereafter, the lipid suspensions were incubated at 0°C for 20 h in the dark to ensure complete hydration of the lipids. The samples were heated to 30°C for 15 min and cooled to 0°C for 1 h. This temperature cycling was repeated one more time to ensure proper mixing of the probes with the host lipid membranes. After more than 24 h of incubation at 0°C, each sample was diluted to less than 50 μg/ml for fluorescence measurements. The sample temperature was regulated by an external water-jet circulator to within ±0.02°C.

Fluorescence measurements

All steady-state fluorescence spectral measurements were performed on a home-built optical multichannel analyzer equipped with a UV-enhanced proximity focused intensified photodiode array IRY-700S detector (Princeton Instrument, Trenton, NJ) attached to a 1/3 m SPEX Minimate 1681 C spectrograph (SPEX Industries, Edison, NJ). A Liconix 4240NB cw UV He-Cd laser (Santa Clara, CA) operating at 325 nm was the excitation source. The fluorescence spectra of $dipy_nPC$ consisted of vibronic bands of monomer and a broad, featureless excimer band (Birks et al., 1963). In this study, *E/M*, defined as the intensity of the excimer peak at 475 nm divided by the intensity of one of the monomer peaks at 392 nm, was measured from each fluorescence spectrum. Using this optical multichannel detection, the uncertainty of a typical *E/M* measurement was well within ±0.01.

All fluorescence intensity decay measurements were performed in the frequency domain on a GREG-200 multifrequency cross-correlation fluorometer (ISS, Champaign, IL) using a Liconix 4240NB cw UV He-Cd laser (Santa Clara, CA) at 325 nm as the excitation source. The operational principle of this multifrequency phase fluorometer has been described in detail elsewhere (Gratton et al., 1984). A typical frequency-domain fluorescence intensity decay data set consisted of phase delays and demodulation ratios of the fluorescence signals with respect to the modulated excitation at different modulation frequencies (0.1–50 MHz) of the excitation (Lakowicz, 1983; Cheng et al., 1994a). For $dipy_nPC$, fluorescence intensity decay measurements were performed at both monomer (392 nm) and excimer (475 nm) emissions. For pyr_nPC, no excimer peak was detected, and intensity decay measurements were made only at monomer emission. The method of calculating the single monomer fluorescence lifetime of pyr_nPC and the decay rate constant of monomer (k_m) from the frequency domain fluorescence intensity decay data has been described previously (Chen et al., 1992; Cheng et al., 1994a).

Calculation of excited-state reaction kinetic parameters of two- and three-state kinetic models from frequency-domain intensity decay and *E/M* data

Based on both the two-state Birks (Birks et al., 1963) and the three-state lattice (Sugar et al., 1991a) kinetic models, various excited-state reaction kinetic parameters of the conjugated pyrene moieties in dipy$_n$PC were calculated from the frequency domain and *E/M* data using a global analysis method that has been described extensively elsewhere (Liu et al., 1993; Cheng et al., 1994a). A brief summary of the two excited-state reaction kinetic models and various definitions of the kinetic parameters is presented here.

For the two-state Birks model, there are two excited-state species of dipy$_n$PC, monomer (M*), and excimer (D*). As shown in Fig. 1, the pyrenyl chains are separated, or in a splay conformation, in the M* state. Only a single step is required for the pyrenyl chains to come close and form an intramolecular pyrene excimer. In the D* state, the pyrenyl chains are assumed to be in all-*trans* conformations (Eklund et al., 1992). The major excited-state kinetic parameters in this two-state model are k_{dm} and k_{md}, representing the forward or association rate constant of the formation of D* and the dissociation rate constant of D*, respectively. Note that M* and D* can decay back to the same ground-state M with corresponding decay rate constants of k_m and k_d. Another kinetic parameter involved in the kinetic model is k_{fd}/k_{fm}, which is defined as the ratio of the intrinsic decay constants of D* and M*. From the measured intensity decays and *E/M* of dipy$_n$PC, k_{dm}, k_{md}, k_d, and k_{fd}/k_{md} can be calculated. On the other hand, k_m can be determined independently from the pyr$_n$PC decay measurements as described above.

For the three-state lattice model, there are three excited-state species of dipy$_n$PC, M*, aggregated (A*), and D*, as shown in Fig. 1. The A* state refers to the configurations in which pyrene moieties are in close apposition. A single rotation of one of the conjugated pyrenes is required to form the D* state. The aggregated configuration of pyrenyl chains can also exist in the ground state (A) and can be directly excited to form A* (Sugar et al., 1991a; Cheng, 1994). The major excited-state kinetic parameters in this

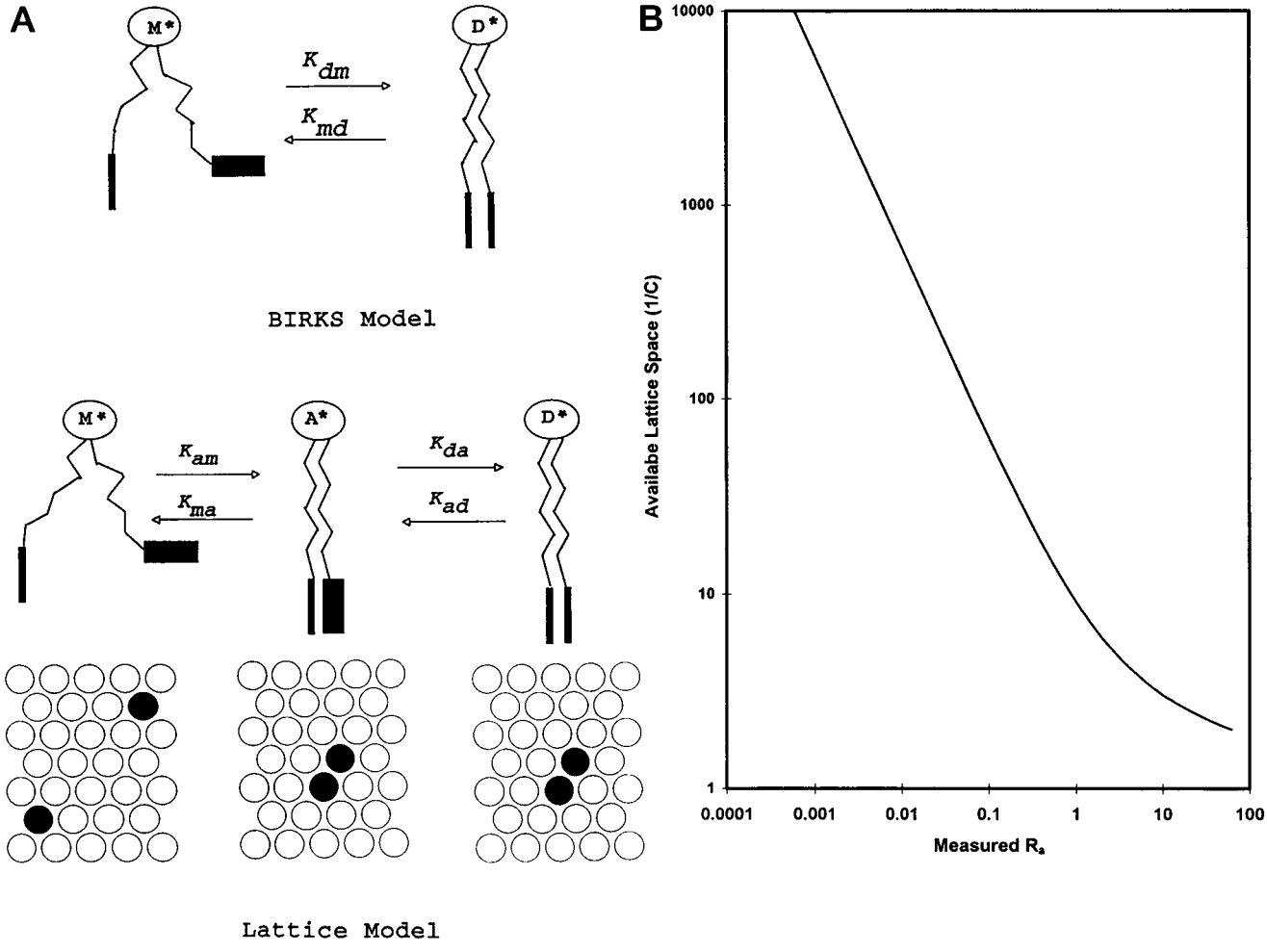

FIGURE 1 (A) Schematic representation of the excited state reactions of dipyrenyl lipids in lipid layers. Both the two-state BIRKS and three-state lattice models are shown. For the BIRKS model, the kinetic parameters k_{dm} and k_{md} refer to the first-order excimer association and dissociation rate constants of the pyrene excimer (D*), respectively. For the lattice model, k_{am} and k_{ma} are the association and dissociation rate constants of the aggregated state (A*), and k_{da} and k_{ad} are the association and dissociation rate constants of D*. The available conformational states of the conjugated pyrenes are represented by a discrete number of lattice points. The two filled circles denote a particular set of conformation of the conjugated pyrenes. The movement of filled circles represents the translational kinetics of pyrenes. In the A* state, the filled circles are shown as closest neighbors. This corresponds to the pyrenyl chains of similar configurations. Here the probable all-*trans* conformations of the pyrenyl chains are shown. The relative orientation of the two conjugated pyrenes may not favor the excimer formation. A single rotational step brings the closely apposed pyrenes to a near-perfect alignment and results in D* formation. (*B*) Dependence of available lattice space (1/*C*) on the measured ratio of aggregated to monomeric states (R_a) as predicted by the lattice model.

three-state model are k_{da}, k_{ad}, k_{am}, and k_{ma}, representing the association rate constant of D*, the dissociation rate constant of D*, the association rate constant of A*, and the dissociation rate constant of A*, respectively. These excited-state kinetic parameters can be calculated from the measured intensity decays and *E/M* of dipy$_n$PC,.

In principle, the lattice model (Sugar et al., 1991a) assumes that each configuration of dipy$_n$PC has a similar probability, and only similar configurations of the pyrenyl chains result in excimer formation. This implies that the intramolecular excimer of dipy$_n$PC may be formed when the pyrenyl chains are in all-*trans* conformations or have identical *gauche* rotamers. Previous fluorescence data (Eklund et al., 1992) of dipy$_n$PC (equal chain length of *n*) as well as dipy$_{n,m}$PC (unequal chain lengths of *n* and *m*) have suggested that intramolecular excimers are formed only when conjugated pyrenes are in "near"-perfect alignment and depend on the chain length of the labeled chains. Because of the stringent alignment requirement and the anisotropic nature of the membranes, it is very likely (Eklund et al., 1992) that most of the excimers are formed by pyrenyl chains in all-*trans* conformations. More detailed photophysical studies are necessary to establish the preferred configurations of intramolecular excimer of dipy$_n$PC in membranes.

Quantitation of EFE and estimation of intramolecular dynamics parameters of dipy$_n$PC

The EFE of dipy$_n$PC can be evaluated by either steady-state *E/M* or time-resolved k_{dm}/k_{md} parameters. Those *E/M* and k_{dm}/k_{md} parameters also serve as first-order approximations to assess the kinetic behavior of conjugated pyrenes in host lipid membranes.

Useful intramolecular conformational and dynamics parameters of dipy$_n$PC can be extracted from the excited-state kinetic parameters. According to the lattice model (Sugar et al., 1991a), the available configurational space for the conjugated pyrene molecules in dipy$_n$PC can be represented by a discrete number of lattice points, as shown in Fig. 1. Each lattice point represents a possible physical location of the conjugated pyrenes. The effective concentration of pyrenes occupying the lattice space is denoted by *C*. Because the number of conjugated pyrene molecules in a single dipyrenyl lipid is only 2, $1/C$ represents the available lattice space or accessible volume of pyrenes in dipy$_n$PC. A conformational parameter R_a, defined as the ratio of the A* and M* states (or A and M ground states) or the equilibrium constant of A* (or A) state, can also be determined from *C*, as shown in the Appendix. Fig. 1 *B* shows the inverse relationship between $1/C$ and R_a based on the theoretical prediction of the lattice model. The transition rate, i.e., the translational rate of pyrenes, is denoted by *f*. The single step rotation of pyrene in the A* state is represented by k'_{dm}. This single rotation event occurs when the pyrenyl chains are close to each other, most probably in the all-*trans* configurations. As shown in the Appendix, all of the parameters, $1/C$, k'_{dm}, *f*, and R_a, can be determined from the recovered excited state kinetic parameters k_{da}, k_{am}, and k_{ma}. Here $1/C$ and R_a are the conformational parameters, and *f* and k'_{dm} are the internal dynamics parameters of dipy$_n$PC.

RESULTS

Steady-state fluorescence spectral measurements of dipy$_n$PC

Steady-state fluorescence spectra of dipy$_n$PC (n = 4, 6, 8, 10, 12, or 14) in DOPE or DOPC were acquired as a function of temperature (T = 0–30°C). The values of *E/M* were subsequently determined from the spectra and are shown in Fig. 2. These steady-state fluorescence parameters were used to quantify the EFE of dipy$_n$PC. For DOPE (n = 4–8) and DOPC (n = 4–14), *E/M* increased steadily with T. However, for DOPE (n = 10–14), a progressive decline in *E/M* with T, starting at ~10°C and ending at ~18°C, was found. The above transition is more evident in Fig. 2 *C*, in which the difference parameter $\Delta E/M$, defined as *E/M* for DOPE minus *E/M* for DOPC, for each n is plotted against T. The distinct advantage of using the "difference" parameter of the same set of probes in two different membranes is that any complex contributions from the intrinsic n and T dependence of the probe fluorescence (Eklund et al., 1992) itself can essentially be eliminated. Consequently, "lipid-matrix" specific structural and/or dynamics properties, as well as their transverse distributions, can be more clearly revealed. Here a sigmoidal behavior of $\Delta E/M$ with transition centered at ~12°C was observed for the longer chain dipy$_n$PC (n = 12, 14), but not for the shorter ones. The above *E/M* and $\Delta E/M$ transition temperature agree with the known first-order inverted hexagonal-lamellar liquid crystalline (L_α-to-H_{II}) phase transition temperature of DOPE based on x-ray diffraction measurements (Gruner et al., 1988). DOPC has no known phase transition within the temperature range 0–30°C.

To compare and quantify the complicated n and T dependence of EFE in two different DOPE and DOPC matrixes, *E/M* (Fig. 3, *A* and *B*) and $\Delta E/M$ (Fig. 3 *C*) were also represented in three-dimensional contour plots. Here a sharp bend, or a change in the slope of contour bands, was clearly found at n = 8 for DOPC (Fig. 3 *A*). For DOPE, the bend at n = 8 was prominent at low temperatures (0–15°C), but less so at higher temperatures. Fig. 3 *C* shows the contour plot of $\Delta E/M$. The interesting features in this plot are the uniform vertical contours of the low $\Delta E/M$ zone for short n (4–8) at all temperatures, an isolated high $\Delta E/M$ zone at low temperatures (0–10°C) and long n (10–14), and an isolated low $\Delta E/M$ zone at high temperatures (20–30°C) and long n (10–14). The above features indicate that i) the EFE of dipy$_n$PC in DOPE is always lower than EFE in DOPC for short n at all temperatures, ii) the EFE for DOPE is higher than the EFE for DOPC for long n and low temperatures (where DOPE and DOPC are both in the L_α phase), and iii) the EFE for DOPE is smaller than the EFE for DOPC for long n at high temperatures (where DOPE is in the H_{II} phase, whereas DOPC remains at the L_α phase). The above observations suggest that significant changes in the EFE may occur when $n \approx 8$ and T = 10–20°C. This intriguing n and T dependence of EFE is also presented in the graphs of *E/M* (Fig. 4, *A* and *B*) and $\Delta E/M$ (Fig. 4 *C*) versus n at three selected temperatures, 4.5°C, 18°C, and 28°C. Here the bends in the contour plots at n = 8 are reflected as kinks in the *E/M* plots and near-zero points in the $\Delta E/M$ plot. Judging from the uncertainties shown in Fig. 4 *C*, the differences in EFE among the three zones (i.e., n = 4–6, $T < 10$°C; $n > 8$, T = 1–10°C; and $n > 8$, T = 20–30°C) were all statistically significant.

Determinations of first-order excited-state kinetic parameters (k_{dm}, k_{md}) of dipy$_n$PC based on the two-state Birks model

Besides steady-state fluorescence measurements, first-order excited-state kinetic parameters of dipy$_n$PC in DOPE and

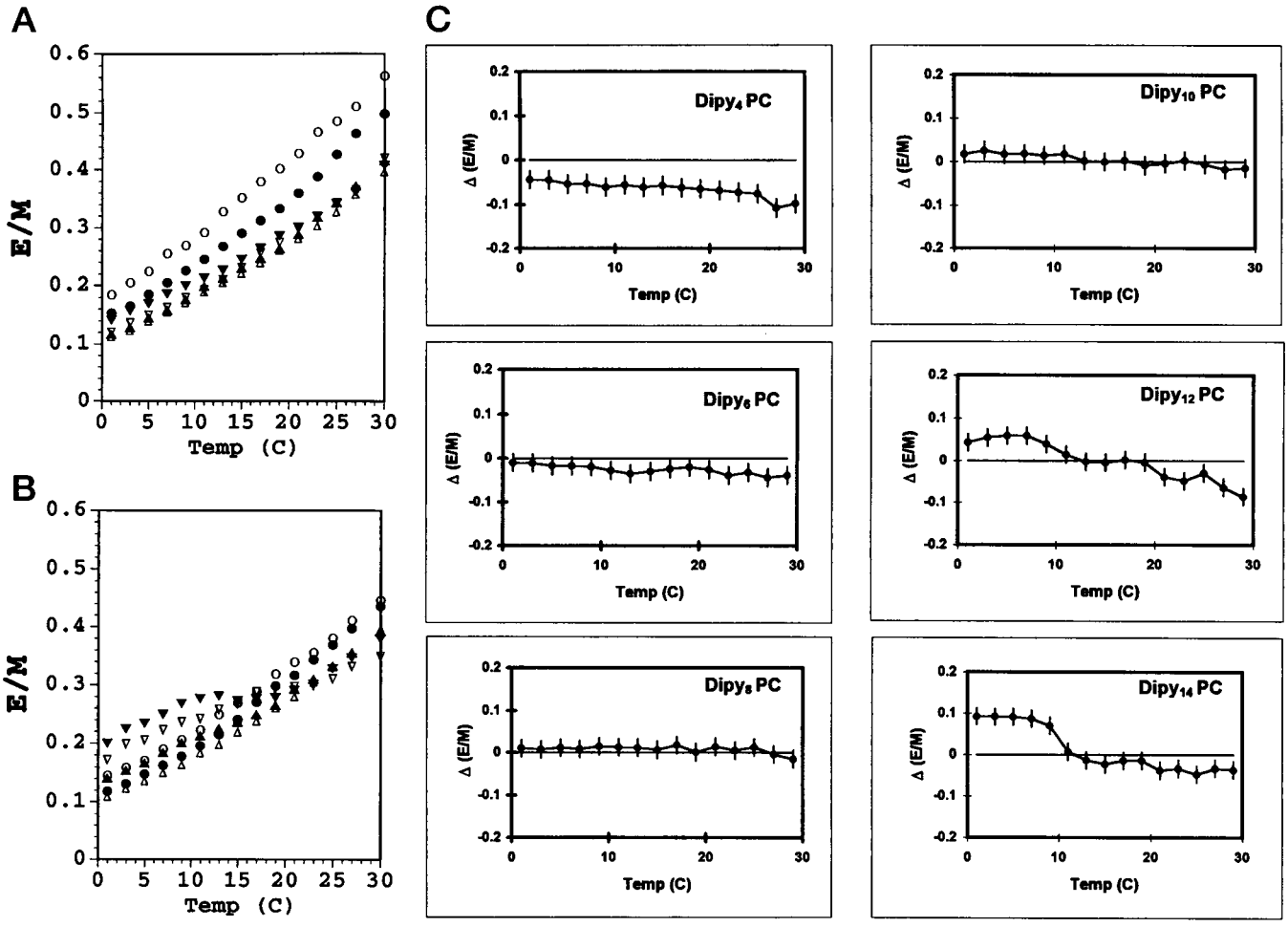

FIGURE 2 Plots of *E/M* of dipy$_n$PC in DOPE (*A*) and DOPC (*B*) versus temperature. The symbols refer to dipy$_4$PC (○), dipy$_6$PC (●), dipy$_8$PC (△), dipy$_{10}$PC (▲), dipy$_{12}$PC (▽), and dipy$_{14}$PC (▼). The difference parameter $\Delta(E/M)$ (*C*), defined as *E/M* for DOPE minus *E/M* for DOPC, versus temperature for each n is also shown. Bars indicate uncertainties in the *E/M* measurements.

DOPC were also determined at 4.5°C, 18°C, and 28°C to further quantify EFE.

Using a two-state Birks model (Fig. 1), four kinetic parameters, k_{dm}, k_{md}, k_d, and k_{fd}/k_{fm}, of dipy$_n$PC were calculated from the frequency-domain and *E/M* data using a global analysis procedure (Sugar, 1991; Cheng et al., 1994a). The excited-state kinetic parameters, k_{dm} and k_{md}, were found to be sensitive to both n and T, whereas k_d and k_{fd}/k_{fm} were only sensitive to T for both DOPE and DOPC. In all cases, k_{dm} was always several times higher than k_{md} for each n. Table 1 shows the representative recovered kinetics parameters (k_{dm}, k_{md}, k_d, and k_{fd}/k_{fm}) for n = 6, 10, and 14 in DOPC at 18°C. The upper and lower confidence limits of the recovered parameters (Ameloot et al., 1986; Cheng et al., 1994a) are also shown. Here, k_{dm} was about fourfold higher than k_{md}. Because of the lack of sensitivity of k_d and k_{fd}/k_{fm} with n and lipid composition, confined fits (keeping those two parameters constant for all of the data sets with the same T during the χ^2 minimization) were also performed (Cheng et al., 1994a,b). Because of the restricted degrees (Davenport et al., 1986; Chen et al., 1992) of freedom during the confined fits, the confidence intervals of the recovered kinetic parameters were narrower than those without the confinement (Table 1). Interestingly, the recovered parameters from the confined fits were always identical to those from the free fits within the confidence limits, as were the χ^2 values. These facts indicate that the values recovered from the two types of fit are of similar quality (Ameloot et al., 1986; Davenport et al., 1986; Cheng et al., 1994a) and therefore reflect the intramolecular dynamics of pyrene molecules in the membranes.

The excited-state kinetic parameter ratio k_{dm}/k_{md} provides a more meaningful and unequivocal way to evaluate EFE than does *E/M*. This is because *E/M* contains contributions of decay rate constants, such as k_{fd}/k_{fm} and k_d, other than excited-state reaction kinetic parameters (Sugar, 1991; Cheng et al., 1994a). One may assume that k_{dm} and k_{md} approximate the "association" and "dissociation" rate constants of the A* state (Sugar, 1991; Cheng et al., 1994a) and that excimer can be formed instantaneously from this A* state, i.e., k_{da} is very large when compared with k_{dm} or k_{md}. Based on these assumptions, k_{dm}/k_{md} may be interpreted as

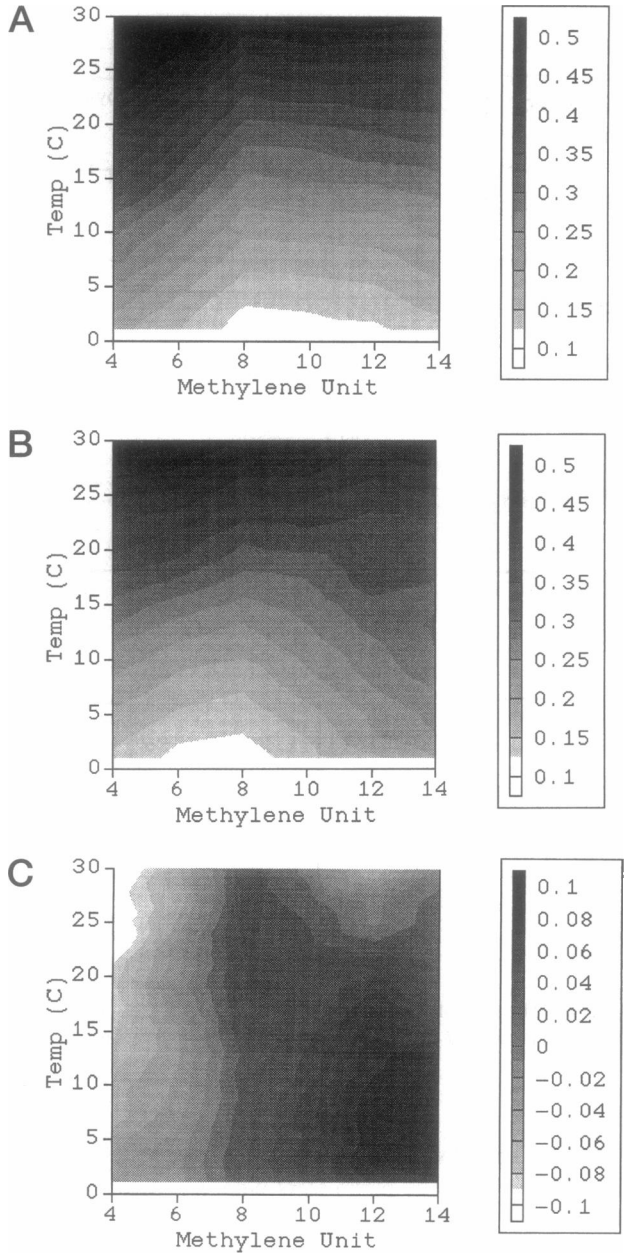

FIGURE 3 Three-dimensional contour plots of *E/M* versus temperature (*vertical axis*) and methylene units *n* (*horizontal axis*) for dipy$_n$PC in DOPC (*A*) and DOPE (*B*). A similar contour plot of the difference parameter $\Delta(E/M)$ (= *E/M* for DOPE minus *E/M* for DOPC) is shown in *C*. The association of the numerical values of *E/M* or $\Delta(E/M)$ with the gray scales is also shown.

the first-order approximation of R_a, the equilibrium constant of A (see Fig. 1). The calculated values of k_{dm}/k_{md} in DOPE and DOPC at T = 4.5°C, 18°C, and 28°C, and the corresponding difference parameter, $\Delta k_{dm}/k_{md}$, are plotted against n in Fig. 4. For clarity, the upper and lower limits of the kinetic parameters are not shown, and the representative values are shown in Table 1. For DOPC, k_{dm}/k_{md} generally decreased with n and T, with noticeable kinks starting at n = 8. For DOPE and $n > 8$, a different trend, i.e., a significant increase in k_{dm}/k_{md} with n, was clearly observed at 4.5°C. At T = 18 and 28°C, the trend of decreasing k_{dm}/k_{md} with n was again observed. The plot of $\Delta k_{dm}/k_{md}$ indicates that i) k_{dm}/k_{md} for DOPE is always lower than k_{dm}/k_{md} for DOPC at all temperatures for n = 4 and 6, ii) k_{dm}/k_{md} for DOPE is higher than k_{dm}/k_{md} for DOPC for $n >$ 8 at low temperature (T = 4.5°C), and iii) k_{dm}/k_{md} for DOPE is lower than k_{dm}/k_{md} for DOPC for $n > 8$ at high temperature (T = 28°C). These three features are identical to those of the independent *E/M* measurements (Fig. 4 *C*) and agree qualitatively with the nature of the three distinctive $\Delta E/M$ zones (Fig. 3 *C*).

Determinations of higher order excited-state kinetic parameters (k_{am}, k_{ma}, k_{da}, and k_{ad}) based on the three-state lattice model

Higher order excited-state kinetic parameters were also recovered from the frequency domain and *E/M* data using a global analysis method (Sugar et al., 1991a; Cheng et al., 1994a). Table 2 shows the representative recovered parameters for n = 6, 10, and 14 in DOPC at 18°C. Similar to k_{dm} and k_{md} obtained from the Birks model, the forward rate constant k_{da} was several times higher than the reverse rate constant k_{ad}. In addition, k_{ad} was independent of n and changed only slightly with T. Using confined fits (keeping the values of k_{da} fixed for all data sets at a fixed T during the χ^2 minimization), k_{da}, k_{am}, and k_{ma} were calculated. Similar to the confined fits based on the Birks model, the recovered parameters within the confidence limits and χ^2 values from these confined fits were similar to those from the free fits. The confidence limits of the recovered parameters from confined fits were again narrower than those of the free fits (Table 2). In most cases, the χ^2 values from three-state fits were significantly lower than those from two-state fits (Tables 1 and 2).

Calculations of lattice parameters (k'_{dm}, f, R_a) from the excited-state kinetic parameters

Based on the higher order excited-state kinetic parameters (k_{da}, k_{am}, k_{ma}), lattice parameters (k'_{dm}, f, R_a), which are associated with the internal rotational and translational mobility and splay conformation, respectively, of the conjugated pyrenes were calculated (see Materials and Methods and Appendix). Here k'_{dm} and f were in the range of 30–200 $\times 10^7$ s^{-1} and were considerably larger than k_{am} or k_{ma}. The values of the intramolecular free volume parameter $1/C$ were around 2–10. As a result, the calculated R_a falls into the range of 1–15 (Fig. 1 *B*). Table 2 demonstrates some representative calculations for n = 6, 10, and 14 in DOPC at 18°C. Because $1/C$ and R_a refer to the same splay conformational property of dipy$_n$PC and are inversely related to each other, only R_a values are presented. Fig. 5 shows the plots of lattice parameters of dipy$_n$PC versus n at 4.5°C,

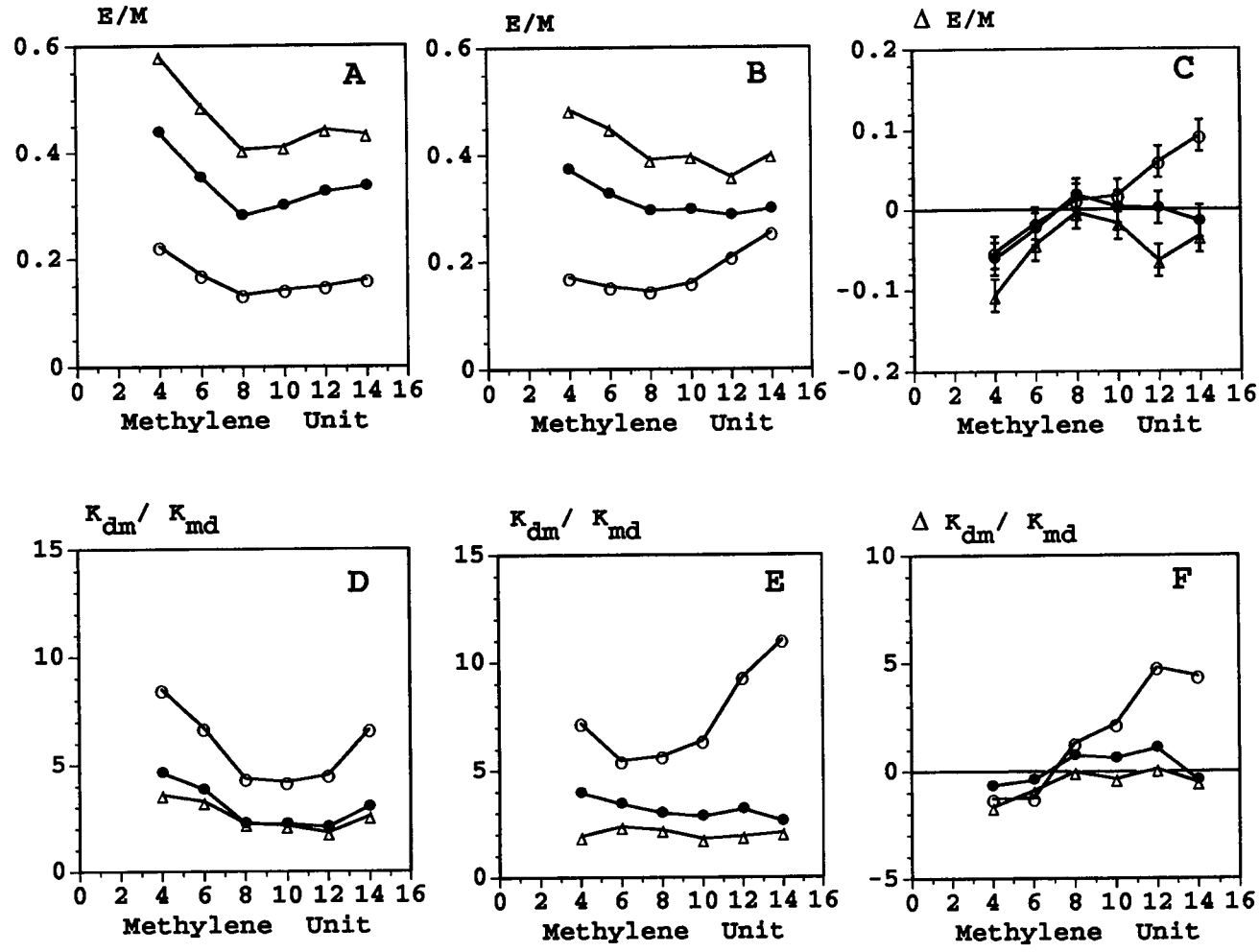

FIGURE 4 Plots of EFE of dipyrenyl lipids in DOPC (*A* and *D*) and DOPE (*B* and *E*) as a function of methylene units *n* of dipy$_n$PC at three representative temperatures, 4.5°C (○), 18°C (●), and 28°C (△). Here EFE is represented by either *E/M* or k_{dm}/k_{md}. The difference parameters Δ *E/M* (*C*) and $\Delta k_{dm}/k_{md}$ (*F*) are also shown.

18°C, and 28°C. For DOPC (Fig. 5 *A*), R_a exhibited a similar trend of *n* dependence as k_{dm}/k_{md} (Fig. 4 *D*). Both k'_{dm} and *f* (Fig. 5, *A* and *D*) showed a prominent peak at $n = 10$ when $T = 18$°C and 28°C. For DOPE (Fig. 5 *H*), R_a has an identical trend of *n* dependence as k_{dm}/k_{md} (Fig. 4 *E*). Instead of a prominent peak at $n = 10$ observed for DOPC, a sharp dip at $n = 8$ was evident for both k'_{dm} and *f* (Fig. 5, *B* and *E*) at 28°C (where DOPE is in the H_{II} phase). Difference parameters, i.e., $\Delta k'_{dm}$, Δf, and ΔR_a, are also shown in Fig. 5, *C*, *F*, and *J*, respectively. Again, ΔR_a showed the same trend of *n* dependence as $\Delta k_{dm}/k_{md}$ (Fig. 4 *F*) and Δ*E/M* (Fig. 4 *C*) at $T = 4.5$°C. An interesting feature was found in R_a and k'_{dm} at $n = 4$ and 6, when $T = 28$°C as demonstrated in $\Delta k'_{dm}$ and ΔR_a plots. Here R_a for DOPE was significantly lower than R_a for DOPC, and k'_{dm} for DOPE was significantly higher than k'_{dm} for DOPC. These observations indicate that the short dipyrenyl chains of dipy$_n$PC in DOPE tend to prefer the splay conformation with signif-

TABLE 1 Representative recovered kinetic parameters (k_{dm}, k_{md}, k_d, k_{fd}/k_{fm}) for dipy$_n$PC in DOPC at 18°C obtained from the two-state Birks model

Parameters	$n = 6$	$n = 6$	$n = 10$	$n = 14$
k_{dm} (10^7 s^{-1})	8.35 (7.10, 9.64)	8.72 (6.22, 9.57)	7.50 (6.82, 8.26)	14.9 (14.3, 15.7)
k_{md} (10^7 s^{-1})	2.38 (2.00, 2.81)	2.27 (2.04, 2.51)	3.38 (2.98, 3.83)	4.93 (4.62, 5.27)
k_d (10^7 s^{-1})	2.03 (1.82, 2.23)	1.90	1.90	1.90
k_{fd}/k_{fm}	0.16 (0.12, 0.19)	0.15	0.15	0.15
k_{dm}/k_{md}	3.55 (2.53, 4.82)	3.84 (3.21, 4.63)	2.22 (1.78, 2.77)	3.02 (2.71, 3.40)
χ^2	2.29	2.26	5.62	1.47

For the confined fit, k_{fd}/k_{fm} and k_d were fixed during the fitting. Values in parentheses represent confidence intervals. The χ^2 value of each fit is also shown.

TABLE 2 Representative recovered kinetic parameters (k_{da}, k_{ad}, k_{am}, k_{ma}) for dipy$_n$PC in DOPC at 18°C obtained from a three-state model

Parameters	$n = 6$	$n = 6$	$n = 10$	$n = 14$
k_{da} (10^7 s^{-1})	15.0 (12.5, 19.8)	14.0 (11.8, 16.9)	24.1 (15.6, 36.9)	22.3 (19.8, 24.8)
k_{ad} (10^7 s^{-1})	2.20 (1.84, 2.92)	2.00	2.00	2.00
k_{am} (10^7 s^{-1})	3.64 (2.59, 5.71)	3.11 (2.62, 3.66)	1.96 (1.70, 2.23)	1.39 (1.20, 1.58)
k_{ma} (10^7 s^{-1})	1.18 (0.50, 2.54)	0.90 (0.43, 1.50)	1.78 (1.30, 2.52)	0.49 (0.32, 0.64)
$1/C$	4.76 (2.94, 9.09)	4.55 (3.22, 6.67)	9.09 (6.67, 12.5)	5.00 (4.00, 6.25)
k'_{dm} (10^7 s^{-1})	54.6 (33.7, 90.8)	49.6 (34.2, 69.8)	109 (64, 181)	82.7 (64.6, 101)
f (10^7 s^{-1})	72.6 (32.5, 211)	58.9 (35.8, 97.3)	69 (46.1, 111)	28.8 (19.7, 40.4)
R_a	3.08 (1.02, 11.4)	3.46 (1.75, 8.51)	1.10 (0.67, 1.72)	2.84 (1.88, 4.94)
χ^2	1.81	1.78	3.60	2.17

For the confined fit, k_{ad} were fixed during the fitting. The lattice parameters, available lattice space ($1/C$), axial rotational rate (k'_{dm}), lattice translational rate (f), and ratio of aggregated state (R_a), calculated from the kinetic parameters, are also shown. Values in parentheses represent confidence intervals. The χ^2 value of each fit is also shown.

icantly higher rotational freedom more than do those in DOPC at $T = 28$°C.

DISCUSSION

EFE and various excited-state kinetic parameters of a series of dipy$_n$PC lipids ($n = 4$ to 14) in the lipid matrix of either DOPE or DOPC have been determined from the steady-state *E/M* and time-resolved fluorescence intensity decay measurements at various temperatures ($T = 0$ to 30°C). By using a three-state lattice model, several lattice parameters relating to the splay conformation (R_a), translational (f), and rotational (k'_{dm}) mobilities of site-selective conjugated pyrene molecules in those lipid matrixes were also calculated. These parameters allowed us to investigate the effects of double bonds and the curvature of lipid matrix on the transverse distributions of conformation and dynamics of site-specific planar molecules with an effective spatial resolution of a few angstroms.

An important issue of any investigations involving transverse distributions of conjugated probe molecules is the precise location of the probes. Previous fluorescence studies (Eklund et al., 1992; Sassaroli et al., 1995) on these pyrene labeled lipids have established that the transverse position of the acyl-linked pyrene molecules is determined solely by the length of the labeled chains. Therefore, by taking into account the finite pyrene size (~4.8 Å), it can be concluded that the center of the conjugated pyrene molecules of the pyrenyl chains should span approximately the C6 to C16 region of the host lipid acyl chains when n is varied from 4 to 14, respectively.

Effects of double bonds on the transverse distribution of EFE and lattice parameters of dipy$_n$PC in DOPC and DOPE bilayer matrix

E/M and k_{dm}/k_{md}, obtained from steady-state and time-resolved fluorescence measurements, respectively, were employed as independent parameters to quantify the EFE of the acyl-linked planar pyrene moieties. The prominent vertical bends, or kinks, observed at $n = 8$ in the *E/M* contour plots of DOPC at all temperatures and of DOPE ($T <$ 10°C), as well as the plots of *E/M* and k_{dm}/k_{md} at certain temperatures, indicate that the conjugated pyrenes positioned at around C10 of the host lipid acyl chains are sensing a structurally and/or dynamically different environment than the other locations of the chains. The distinctive zone boundary in the $\Delta E/M$ contour plot at $n = 8$ further supports this conclusion. Interestingly, the C10 location corresponds well to the position of the *cis* double bonds of the oleoyl acyl chains of DOPC and DOPE. For $T < 10$°C, DOPC and DOPE are in the lamellar L_α phase. In addition, structural measurements (Gruner et al., 1988; Fenske et al., 1990) have confirmed that the lipid monolayer thickness d_b of either lipid matrix is ~18 Å (Fig. 6). Therefore, the deflection of the EFE parameters at $n = 8$ could be due to the localized effects of the rigid (but conformationally disordering) double bonds (Rey et al., 1992; Kodati and Lafleur, 1992; Pearce and Harvey, 1993).

By using the three-state lattice model, the conformational and internal dynamics parameters of dipyrenyl lipids can be resolved separately. The values of R_a for bilayer DOPC and DOPE exhibit prominent and broad minima at around $n = 8$, in agreement with the specific features of EFE parameters observed at $n = 8$. As indicated in Materials and Methods and Fig. 1 *B*, R_a is inversely related to the accessible volume or configurational space ($1/C$) available to the conjugated pyrenes. Therefore, the planar conjugated pyrenes may prefer the splay conformation over the tightly packed aggregated conformation at the vicinity of the localized double bonds of the host bilayer lipid matrix. These disordering effects at around $n = 8$ are more prominent at high temperatures, e.g., a sixfold decline in R_a for DOPC at $T = 28$°C as compared with less than a 50% decrease for either DOPC or DOPE at 4.5°C as n increases from 4 to 8, as shown in Fig. 5.

The proposed localized and disordering effects of double bonds are also confirmed by the internal dynamics parameters. Here k'_{dm} and f, which represent the hindered rotational and translational mobilities of conjugated pyrenes, respectively (Fig. 1), show a prominent and sharp peak (particularly so for k'_{dm}) for $n = 10$ in DOPC at $T = 18$°C

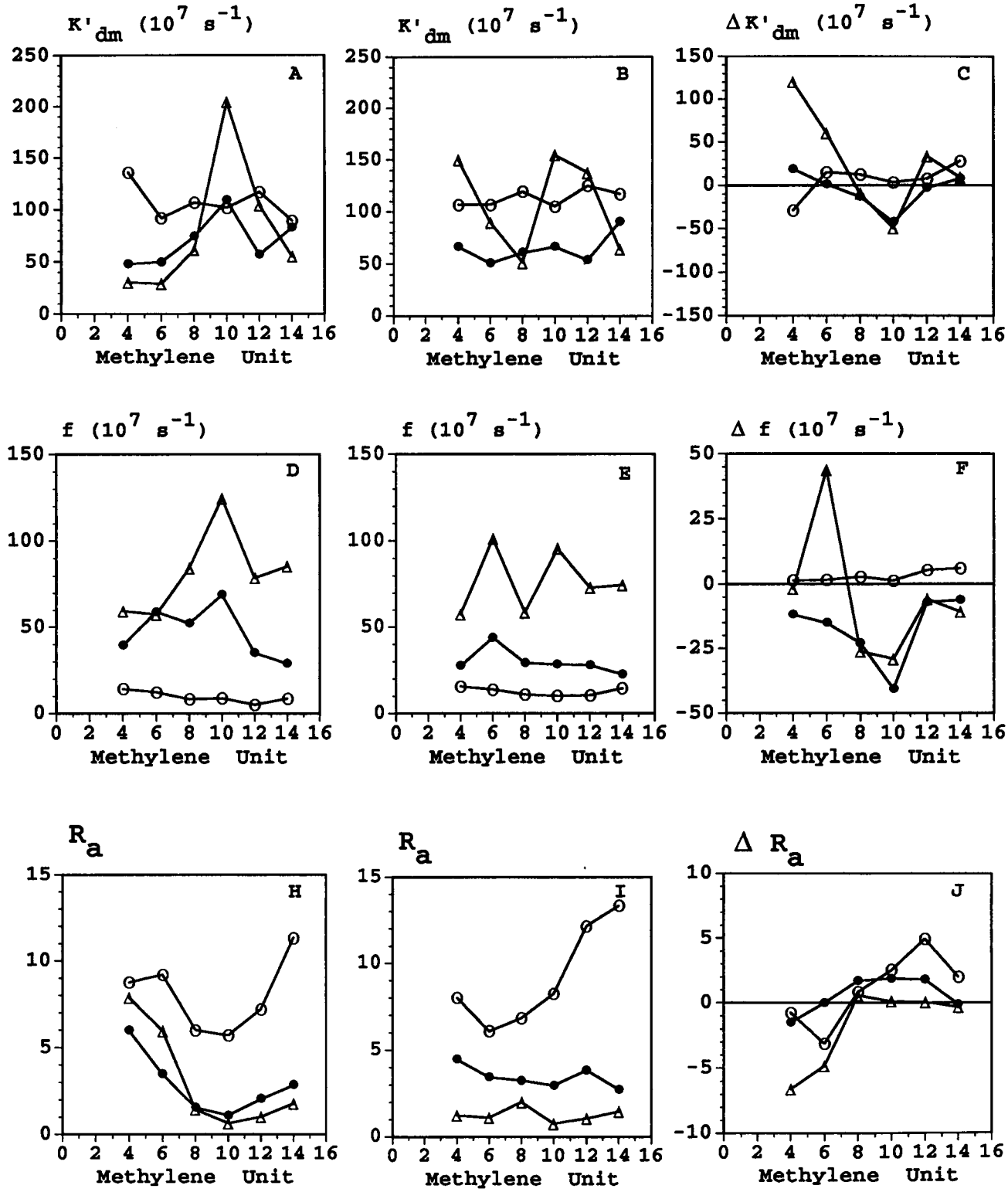

FIGURE 5 Plots of lattice parameters k'_{dm}, f, and R_a of dipyrenyl lipids in DOPC (*A*, *D*, and *H*) and DOPE (*B*, *E*, and *I*), respectively, as a function of methylene units n of dipy$_n$PC at three representative temperatures, 4.5°C (○), 18°C (●) and 28°C (△). Their difference parameters $\Delta k'_{dm}$ (*C*), Δf (*F*), and ΔR_a (*J*) are also shown.

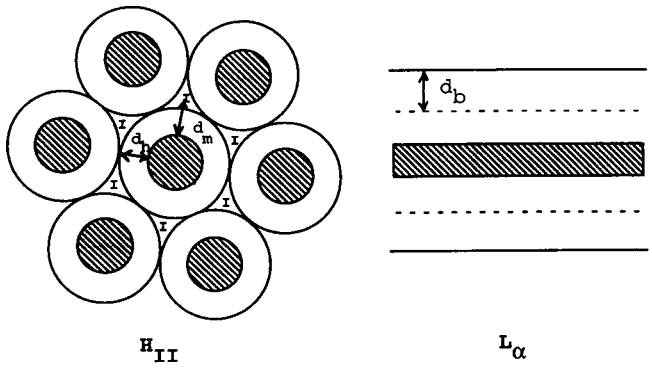

FIGURE 6 Geometrical structures of inverted hexagonal (H_{II}) lamellar liquid crystalline (L_α) phases. The shaded area represents the water phase. In the H_{II} phase, I denotes the interstitial space between the lipid tubes, which may be occupied by presumably stretched chains. The structural parameter d_b represents the estimated thickness of one lipid layer in the L_α phase, and d_h and d_m represent estimated thickness of the lipid cylindrical tubes and the average distance from the lipid headgroup to the center of the interstitial space, respectively, in the H_{II} phase.

and 28°C. This is obviously different from the broad minima around $n = 8$ for R_a as well as EFE parameters. This difference may be related to the fact that k'_{dm} is associated with the single rotational step when the pyrenyl chains are in the A state (Fig. 1). Therefore, this parameter should be more position sensitive than the other lattice parameters. The k'_{dm} or f peak for DOPC, like R_a, exhibits a strong temperature dependence. For example, k'_{dm} increases nearly 10-fold at 28°C, versus a mere twofold increase at 18°C when n increases from 4 to 10.

Effects of curvature on the transverse distribution of EFE and lattice parameters of dipy$_n$PC in DOPC and DOPE matrix

DOPE undergoes a first-order L_α-to-H_{II} phase transition starting at around 10°C. The lipids are arranged essentially in a plane (with large radius of curvature) in the L_α phase, whereas they adopt a highly curved inverted cylindrical form (with radius of curvature on the order of angstroms) in the H_{II} phase. According to the stress model (Seddon, 1990; Gruner, 1992; Hui, 1993), the lipid monolayers of PE in a planar bilayer form (i.e., DOPE at $T < 10$°C) would experience a greater lateral stress, or larger stored bending energy, than do the same PE monolayers in the curved cylindrical form (i.e., DOPE at $T > 20$°C). In contrast, DOPC has negligible curvature associated stress at all temperatures. The site-selective probes used here allow us to examine carefully the effects of the proposed curvature-associated stress on the EFE and lattice parameters of site-selective molecules in both planar bilayer and hexagonally packed cylindrical forms.

The appearance of two distinctive zones ($n > 8$, T = 0–10°C; and $n > 8$, T = 20–30°C) in the $\Delta E/M$ contour plot suggests that only the longer pyrenyl chains ($n > 8$) are sensitive to the curvature-related phase transition of DOPE. They also suggest that, for those long pyrenyl chains, the EFE for DOPE is significantly higher than the EFE for DOPC at low temperatures and that the EFE for DOPE becomes smaller than the EFE for DOPC at high temperatures. Therefore, it is concluded that the structural conformation and/or dynamics of the long pyrenyl chains in curvature-stressed DOPE are distinctively different from those in DOPC (control) when both lipid matrixes are in the planar bilayer form. Moreover, as DOPE transforms to the curvature-relaxed or preferable H_{II} phase (T = 20–30°C), a reverse trend in the structural conformation and/or dynamics of the long pyrenyl chains prevails. The use of lattice parameters further allows us to delineate the contributions of splay conformation and internal dynamics of conjugated pyrenes to the distinctive curvature-stressed (T = 0–10°C) and curvature-relaxed (T = 20–30°C) zones of DOPE.

For the curvature-stress zone (T = 0–10°C) and for $n > 8$, R_a for DOPE is greater than R_a for DOPC. This indicates that the long pyrenyl chains would prefer the aggregated configurations over the splay conformation in the curvature-stress state of DOPE. Interestingly, the internal dynamics parameters, f and k'_{dm}, are not sensitive to the curvature-stress state of DOPE. On the other hand, the lattice parameters of shorter pyrenyl chains ($n < 8$) respond to this curvature-stress rather differently than do the longer pyrenyl chains. Here f and k'_{dm} are quite insensitive to the stress, whereas R_a for DOPE is even slightly smaller than R_a for DOPC. This different behavior of short pyrenyl chains may be explained as follows. The interactions among molecules near the lipid/water interfacial region of PE are probably stronger than those of PC, because of the smaller geometrical size and the interlipid hydrogen bonding capability of the PE headgroup (Epand, 1995 and references therein). The stronger interactions may affect the internal conformations of short pyrenyl chains in such a way that the average penetration depths (or transverse distance) of the two conjugated pyrenes in DOPE are greater than those in DOPC. Previous data strongly suggest that a near-perfect alignment of the pyrene molecules (Lemmetyinen et al., 1989; Sugar, 1991; Eklund et al., 1992) is a necessary condition for the pyrene excimer formation. Alternatively, near the L_α-to-H_{II} phase transition, packing defects (Siegel, 1986; Epand, 1995) near the interfacial regions may be present. Some of the short-chain dipy$_n$PC may partition into those defects where conjugated pyrenes would prefer the splay conformation over the aggregated form.

In the curvature-relaxed zone of DOPE (T = 20–30°C), the conformations of long pyrenyl chains are again quite different from those of short pyrenyl chains. R_a for DOPE is similar to R_a for DOPC for long chains ($n > 8$), but is about sevenfold lower than R_a for DOPC for short pyrenyl chains ($n < 8$). This interesting chain-length dependence could be explained based on the packing geometry of lipid molecules in the H_{II} phase. Fig. 6 shows the proposed geometrical arrangements of lipids in H_{II} and L_α phases (Gruner et al., 1988; Tate and Gruner, 1989). In the one-dimensional L_α phase, the relevant structural parameter for acyl chains is

monolayer thickness d_b (~18 Å for either DOPC or DOPE). However, in the two-dimensional H_{II} phase, two structural parameters for acyl chains are required. They are d_h and d_m, which represent the short and long transverse distances that the acyl chains may occupy, and their values have been estimated (Gruner et al., 1988; Tate and Gruner, 1989) to be 16 and 22 Å, respectively, for DOPE. Previous studies (Seddon, 1990; Steenhuizen et al., 1991; Gruner, 1992) have also suggested that the presence of void in the interstitial I space would contribute to high chain packing free energy. Hence, the acyl chains may have to stretch to fill in those sixfold symmetric interstitial spaces (Steenhuizen et al., 1991; Gruner, 1992) to avoid the formation of a void. Based on the above geometrical considerations, the apparent preference for the splay conformation by the short pyrenyl chains suggests that the site-specific pyrenes have more accessible space in a curved lipid matrix than in a planar lipid matrix. However, in a curved matrix, the accessible space for long pyrenyl chains would be similar to that in a planar matrix. This is because the long pyrenyl chains are able to occupy the I space, whereas short pyrenyl chains are not. Assuming that the headgroup of dipy$_n$PC has a transverse dimension of roughly 3 Å, the transverse distance of dipy$_{14}$PC with acyl chain in all-*trans* configurations will have a transverse length of ~21 Å, which is greater than d_b and similar to d_m. Because of the possibility of adopting the more stretched conformation, the average splay conformation of long pyrenyl chains in a structural heterogeneous curved lipid matrix can be similar to that in a more homogeneous bilayer lipid matrix. Our results also indicate that f and k'_{dm} exhibit a significant dip at $n = 8$ in the H_{II} phase of DOPE. We speculate that this abrupt decrease in mobility of conjugated pyrenes is again due to the presence of double bonds in the host acyl chains. It is upshifted by 2 m.u. as compared to the perturbations at $n = 10$ for DOPC. This shift may result from a decrease in the effective transverse distance of the double bonds due to the host lipid acyl chains in response to the large interfacial curvature of the H_{II} phase.

In conclusion, this systematic fluorescence study on site-specific dipyrenyl lipids provides evidence that the internal dynamics and conformation of conjugated planar pyrene molecules exhibit interesting chain length-dependent behavior in planar and curved lipid matrix. The transverse distributions are quantified in considerable detail by the zone features of *E/M* contour plots, for instance. By using a lattice mode, the responses of the splay conformation and internal dynamic of site-specific molecules to both curvature-stressed and curvature-relaxed lipid matrixes have also been separately explored.

APPENDIX: CALCULATIONS OF LATTICE PARAMETERS FROM RECOVERED EXCITED-STATE REACTION KINETIC PARAMETERS

The excited-state reaction parameters (k_{da}, k_{am}, k_{ma}) depicted by the three-state model (Sugar et al., 1991a; Cheng et al., 1994a) can be calculated from the frequency-domain fluorescence intensity decays of the pyrene monomer and excimer and *E/M* using a global fit in the complex space. These kinetic parameters are further related to the lattice parameters (f, C, k'_{dm}, R_a), as given by the following equations (Sugar et al., 1991a; Liu et al., 1993; Cheng et al., 1994a). Note that prime in the lattice parameter k'_{dm} is used to distinguish it from the k_{dm} used in the Birks model.

$$k_{da} = k'_{dm}C/[1 - (1 - C)^6] \quad \text{(A1)}$$

$$k_{am} = 12fC(1 + C)(C^2 - 3C + 3) \quad \text{(A2)}$$

$$k_{ma} = 12fC(1 - C)^6(C^2 - C^3 - C + 3)/[1 - (1 - C)^6] \quad \text{(A3)}$$

$$R_a = [1/(1 - C)^6] - 1. \quad \text{(A4)}$$

As seen in Eqs. A2 and A3, k_{am}/k_{ma} is a function of C. Using a numerical method, the value of C can be determined from the recovered k_{am}/k_{ma}. Once C is determined, k'_{dm}, f, and R_a can subsequently be determined from Eqs. A1, A3, and A4, respectively.

We thank Digala Kulawansa for performing the steady-state *E/M* fluorescence measurements. We would like to thank Drs. Richard Epand, Sek Wen Hui, Istvan Sugar, and Jorma Virtanen for enlightening discussions. The sincere criticisms of the reviewers on the assumptions of the lattice model and the interpretations of various physical parameters of dipy$_n$PC are gratefully acknowledged. The nonlinear least-squares fit subroutine was kindly provided by Dr. Michael L. Johnson of the University of Virginia.

This work was supported by grants from the Robert A. Welch Foundation (D-1158) and the National Institutes of Health (CA47610) (KHC) and from the Sigrid Juselius Foundation, Finnish Academy (PS).

REFERENCES

Ameloot, M., J. M. Beechem, and L. Brand. 1986. Compartmental modeling of excited-state reactions: identifiability of the rate constants from fluorescence decay surfaces. *Chem. Phys. Lett.* 129:211–219.

Birks, J. B., D. J. Dyson, and I. H. Munro. 1963. "Excimer" fluorescence II. Lifetime studies of pyrene solutions. *Proc. R. Soc. Lond.* 275: 575–588.

Chen, S.-Y., K. H. Cheng, and B. W. Van Der Meer. 1992. Quantitation of lateral stress in lipid layer containing nonbilayer phase preferring lipids by frequency-domain fluorescence spectroscopy. *Biochemistry.* 31: 3759–3768.

Cheng, K. H. 1994. Infrared study of bilayer stability behavior of binary and ternary mixtures containing unsaturated phosphatidylethanolamine. *Chem. Phys. Lipids.* 70:43–51.

Cheng, K. H., L. Ruymgaart, L. Liu, P. Somerharju, and I. P. Sugar. 1994a. Intramolecular excimer kinetics of fluorescent dipyrenyl lipids. 1. DMPC/cholesterol membranes. *Biophys. J.* 67:902–913.

Cheng, K. H., L. Ruymgaart, L. Liu, P. Somerharju, and I. P. Sugar. 1994b. Intramolecular excimer kinetics of fluorescent dipyrenyl lipids. 2. DOPE/DOPC membranes. *Biophys. J.* 67:914–921.

Chiu, S.-W., M. Clark, V. Balaji, S. Subramaniam, H. L. Scott, and E. Jakobsson. 1995. Incorporation of surface tension into molecular dynamics simulation of an interface: a fluid phase bilayer membrane. *Biophys. J.* 69:1230–1245.

Cowsley, S. J., R. H. Templer, and D. R. Klug. 1993. Dipyrenylphosphatidylcholine as a probe of bilayer pressure. *J. Fluorescence.* 3:149–152.

Davenport, L., J. R. Knutson, and L. Brand. 1986. Excited-state proton transfer of equilenin and dihydroequilenin: interaction with bilayer vesicles. *Biochemistry.* 25:1186–1195.

De Loof, H., S. C. Harvey, J. P. Segrest, and R. W. Pastor. 1991. Mean field stochastic boundary molecular dynamics simulation of a phospholipid in a membrane. *Biochemistry.* 30:2099–2113.

Eklund, K. K., J. A. Virtanen, P. K. J. Kinnunen, J. Kasurinen, and P. J. Somerharju. 1992. Conformation of phosphatidylcholine in neat and cholesterol containing crystalline bilayers. Application of a novel method. *Biochemistry.* 31:8560–8565.

Epand, R. M. 1995. Comments on fluorescence methods for probing local deviations from lamellar packing. *J. Fluorescence.* 5:3–8.

Fattal, D. R., and A. Ben-Shaul. 1994. Mean-field calculations of chain packing and conformational statistics in lipid bilayers: comparison with experiments and molecular dynamics studies. *Biophys. J.* 67:983–995.

Fenske, D. B., H. C. Jarrell, Y. Guo, and S. W. Hui. 1990. Effect of unsaturated phosphatidylethanolamine on the chain order profile of bilayer at the onset of the hexagonal phase transition. A 2H NMR study. *Biochemistry.* 29:11222–11229.

Galla, H. J., and E. Hartman. 1980. Excimer forming lipids in membrane research. *Chem. Phys. Lipids.* 27:199–219.

Gratton, E., D. M. Jameson, and R. D. Hall. 1984. Multifrequency phase and modulation fluorometry. *Annu. Rev. Biophys. Bioeng.* 13:105–124.

Gruner, S. M. 1992. Nonbilayer lipid phases. *In* The Structure of Biological Membranes. P. Yeagle, editor. CRC Press, Boca Raton, FL. 211–250.

Gruner, S. M., M. W. Tate, G. L. Kirk, P. T. C. So, D. C. Tyrner, and D. T. Keane. 1988. X-ray diffraction study of the polymorphic behavior of *N*-methylated dioleoylphosphatidylethanolamine. *Biochemistry.* 27: 2852–2866.

Heimburg, T., P. Hilderbrandt, and D. Marsh. 1991. Cytochrome C-lipid interactions studied by resonance Raman and ^{31}P NMR spectroscopy. Correlation between the conformational changes of the protein and the lipid bilayer. *Biochemistry.* 30:9084–9089.

Hresko, R. C., I. P. Sugar, Y. Barenholz, and T. E. Thompson. 1987. The lateral distribution of pyrene-labeled sphingomyline and gluocosylceramide in phosphatidylcholine bilayer. *Biophys. J.* 51:725–733.

Hui, S. W. 1993. Lipid molecular shape and high curvature structures. *Biophys. J.* 65:1361–1362.

Israelachvilli, J. N., D. J. Mitchell, and B. W. Ningham. 1977. Theory of self-assembly of lipid bilayers and vesicles. *Biochim. Biophys. Acta.* 470:185–201.

Keller, S. L., S. M. Bezrukov, S. M. Gruner, M. W. Tate, I. Vodyanoy, and V. A. Parsegian. 1993. Probability of alamethicin conductance states varies with nonlamellar tendency of bilayer phospholipids. *Biophys. J.* 65:23–27.

Kodati, V. R., and M. Lafleur. 1992. Comparison between orientational and conformational orders in fluid lipid bilayers. *Biophys. J.* 64: 163–170.

Lafleur, M., P. R. Cullis, B. Fine, and M. Bloom. 1990. Comparison of the orientational order of lipid chains in L_α-H_{II} phases. *Biochemistry.* 29: 8325–8333.

Lakowicz, J. R. 1983. Principle of Fluorescence Spectroscopy. Plenum Press, New York.

Lemmetyinen, H., M. Yliperttula, J. Mikkola, J. A. Virtanen, and P. K. J. Kinnunen. 1989. Kinetic study of monomer and excimer fluorescence of pyrene-substituted phosphatidylcholine in phosphatidylcholine bilayers. *J. Phys. Chem.* 93:7170–7175.

Lentz, B. R., G. F. McIntyre, D. J. Parks, J. C. Yates, and D. Massenburg. 1992. Bilayer curvature and certain amphipaths promote poly(ethylene glycerol)-induced fusion of dipalmitoylphosphatidylcholine unilamellar vesicles. *Biochemistry.* 31:2643–2653.

Lewis, N. A. H., R. N. McElhaney, P. E. Harper, D. C. Turner, and S. M. Gruner. 1994. Studies of the thermotropic phase behavior of phosphatidylcholines containing 2-alkyl substituted fatty acyl chains: a new class of phosphatidylcholines forming inverted nonlamellar phases. *Biophys. J.* 66:1088–1103.

Liu, L., K. H. Cheng, and P. Somerharju. 1993. Frequency-resolved intramolecular excimer fluorescence study of lipid bilayer and nonbilayer phases. *Biophys. J.* 64:1869–1877.

Pearce, L. L., and S. C. Harvey. 1993. Langevin dynamics studies of unsaturated phospholipids in a membrane environment. *Biophys. J.* 65:1084–1092.

Rey, A., A. Kolinski, J. Skolnick, and Y. K. Levine. 1992. Effect of double bonds on the dynamics of hydrocarbon chains. *J. Chem. Phys.* 92: 1240–1249.

Sassaroli, M., M. Ruonala, J. Virtanen, M. Vauhkonen, and P. Somerharju. 1995. Transversal distribution of acyl-linked pyrene moieties in liquid crystalline phosphatidylcholine bilayers. A fluorescence quenching study. *Biochemistry.* 34:8843–8851.

Sassaroli, M., M. Vauhkonen, P. Somerharju, and S. Scarlata. 1993. Diphenylphosphatidylcholines as membrane fluidity probe. Pressure and temperature dependence of the intramolecular rate. *Biophys. J.* 64: 137–149.

Seddon, J. M. 1990. Structure of the inverted hexagonal (H_{II}) phase, and non-lamellar transitions of lipids. *Biochim. Biophys. Acta.* 1031:1–69.

Seelig, J., and N. Waespe-Šarčević. 1978. Molecular order in *cis* and *trans* unsaturated phospholipid bilayers. *Biochem. J.* 17:3310–3315.

Siegel, D. P. 1986. Inverted micellar intermediates and the transitions between lamellar, cubic and inverted hexagonal phases. II. Implications for membrane-membrane interactions and membrane fusion. *Biophys. J.* 49:1171–1183.

Slater, S. J., F. J. Taddeo, and C. Ho. 1994. The modulation of protein kinase C activity by membrane lipid bilayer structure. *J. Biol. Chem.* 269:4866–4871.

Steenhuizen, L., D. Kramer, and A. Ben-Shaul. 1991. Statistical thermodynamics of molecular organization in the inverse hexagonal phase. *J. Phys. Chem.* 95:7477–7483.

Sugar, I. P. 1991. Use of fourier transforms in the analysis of fluorescence data. 1. A general method for finding explicit relationships between photophysical models and fluorescence parameters. *J. Phys. Chem.* 95:7508–7515.

Sugar, I. P., J. Zeng, and P. L.-G. Chong. 1991a. Use of Fourier transforms in the analysis of fluorescence data. 3. Fluorescence of pyrene-labeled phosphatidylcholine in lipid bilayer membrane. A three-state model. *J. Phys. Chem.* 95:7524–7534.

Sugar, I. P., J. Zeng, M. Vauhkonen, P. Somerharju, and P. L.-G. Chong. 1991b. Use of fourier transforms in the analysis of fluorescence data. 2. Fluorescence of pyrene-labeled phosphatidylcholine in lipid bilayer membrane. Test of the Birks model. *J. Phys. Chem.* 95:7516–7523.

Tang, D., and P. L.-G. Chong. 1992. E/M dips evidence for lipid regular distributed into hexagonal super-lattices in pyrene-PC/DMPC binary mixtures at specific concentrations. *Biophys. J.* 63:903–910.

Tate, M. W., and S. M. Gruner. 1989. Temperature dependence of the structural dimensions of the inverted hexagonal (H_{II}) phase of phosphatidylethanolamine-containing membranes. *Biochemistry.* 28:4245–4253.

Thurmond, R. L., G. Lindblom, and M. F. Brown. 1993. Curvature, order, and dynamics of lipid hexagonal phases studied by deuterium NMR spectroscopy. *Biochemistry.* 32:5394–5410.

Vauhkonen, M., M. Sassaroli, P. Somerharju, and J. Eisinger. 1990. Dipyrenylphosphatidylcholines as membrane fluidity probes. Relationship between intramolecular and intermolecular excimer formation rates. *Biophys. J.* 57:291–300.

Wiener, M., and S. H. White. 1992. Structure of a fluid dioleoylphosphatidylcholine bilayer determined by joint refinement of x-ray and neutron diffraction data. III. Complete structure. *Biophys. J.* 61:434–447.

Winterhalter, M., and W. Helfrich. 1992. Bending elasticity of electrically charged bilayers: coupled monolayers, neutral surfaces and balancing stresses. *J. Phys. Chem.* 96:327–330.

Xiang, T. 1993. A computer simulation of free-volume distributions and related structural properties in a model lipid bilayer. *Biophys. J.* 65: 1108–1120.